Quantification of the Conditioning Phase in Cooled Pixelated TlBr Detectors

Will Koehler, Zhong He, *Senior Member, IEEE*, Sean O'Neal, Hao Yang, Hadong Kim, Leonard Cirignano, and Kanai Shah

***Abstract*—Thallium-bromide (TlBr) is currently under investigation as an alternative room-temperature semiconductor gamma-ray spectrometer due to its favorable material properties (large bandgap, high atomic numbers, and high density). Previous work has shown that 5 mm thick pixelated TlBr detectors can achieve sub-1% FWHM energy resolution at 662 keV for single-pixel events. These results are limited to $-20°C$ operation where detector performance is stable. During the first one to five days of applied bias at $-20°C$, many TlBr detectors undergo a conditioning phase, where the energy resolution improves and the depth-dependent electron drift velocity stabilizes. In this work, the spectroscopic performance, drift velocity, and freed electron concentrations of multiple 5 mm thick pixelated TlBr detectors are monitored throughout the conditioning phase. Additionally, conditioning is performed twice on the same detector at different times to show that improvement mechanisms relax when the detector is stored without bias. We conclude that the improved spectroscopy results from internal electric field stabilization and uniformity caused by fewer trapped electrons.**

***Index Terms*—Alternative room temperature semiconductor, TlBr spectrometers.**

I. Introduction

THALLIUM-BROMIDE is an attractive material for room-temperature radiation detection because of its high stopping power and large bandgap. Additionally, the melting point for TlBr is only $460°C$; therefore, simple melt-based techniques like the traveling molten zone (TMZ) method can be used for both growth and purification [1], [2]. Many researchers have shown high resistivity ($10^{10} - 10^{11}\Omega$ cm) and good electron mobility-lifetime products ($\mu\tau_e > 10^{-3}$ cm^2/V) in thick (up to 5 mm) TlBr detectors, resulting in good room-temperature or near room-temperature performance [3]–[7].

Sub-1% FWHM single-pixel energy resolution at 662 keV has been achieved on TlBr devices [3], but these results are mostly limited to $-20°C$ operation. After hours to days of room-temperature operation, the performance degrades as a result of ionic conduction. Experimental results suggest that Tl^+ and Br^- ions accumulate under the cathode and anode electrodes respectively and interact with the contact material. The degradation of the contact material eventually causes device failure [8]–[11].

Reports have shown stable room-temperature operation by applying Tl electrodes [8] and periodically switching the polarity of the bias [4]. Tl is extremely toxic, complicating the electrode fabrication process. Additionally, stable performance for longer than three days has not been experimentally demonstrated. Further study is required to determine whether Tl electrodes can achieve long-term ($>$ month) room-temperature stability. Periodically switching the bias is undesirable for pixelated detectors in which the anode must be the pixelated electrode for optimal signal generation.

To date, the most consistent method to achieve long-term stability ($\sim$ months) is to operate the device at $-20°C$ [3], [7]. During the first one to five days of applied bias at $-20°C$, many TlBr detectors exhibit a so called "conditioning phase," where the energy resolution improves and the depth-dependent electron drift velocity increases and stabilizes. In an effort to understand the cause of the conditioning phase, three TlBr detectors approximately 5 mm thick were monitored at $-20°C$. Our results suggest that the improved spectroscopy and stabilized drift velocity are the result of a more uniform internal electric field. LED interrogation of the sample throughout the conditioning phase suggests that the improved electric field results from the eventual removal of trapped electrons which cause undesirable space charge fields.

II. Methods

A. Experimental Setup

The TlBr detectors tested in this work were approximately 5 mm in each dimension and were fabricated by Radiation Monitoring Devices (RMD). The raw material was purified and grown using the TMZ method [2] and an evaporator was used to apply Au/Cr contacts. Each detector had a three-by-three pixelated anode and a planar cathode. The pixel pad area was 0.9×0.9 mm^2 and the pixel pitch was 1 mm. A 1 mm guard ring surrounded the outer pixels. Signals from all nine anodes and the cathode were read out using eV-Products 509 charge sensitive preamplifiers, whose outputs were digitized using a computer-operated 14 bit GageScope. For most testing scenarios, each of the ten waveforms was recorded in 512 data points sampled every 100 ns for a total sampling window of 51 μs. A Thermotron S-1.2-3200 environmental chamber

Manuscript received February 20, 2015; revised April 09, 2015; accepted June 18, 2015. Date of publication July 22, 2015; date of current version August 14, 2015. This work was supported by DHS DNDO (SBIR contract #HSHQDC-13-C-00068) through RMD and DOE (Award #DE-AC52-07NA27344) through LLNL.

W. Koehler, Z. He, S. O'Neal, and H. Yang are with the Department of Nuclear Engineering and Radiological Sciences, University of Michigan, Ann Arbor, MI 48109 USA (e-mail: koehlerw@umich.edu).

H. Kim, L. Cirignano, and K. Shah are with Radiation Monitoring Devices Inc., Watertown, MA 02472 USA.

Color versions of one or more of the figures in this paper are available online at http://ieeexplore.ieee.org.

Digital Object Identifier 10.1109/TNS.2015.2448420

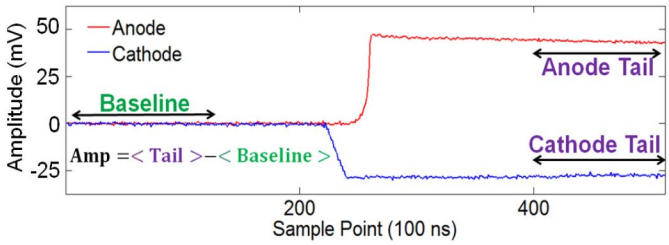

Fig. 1. Signal amplitudes were determined using 100-point simple subtraction.

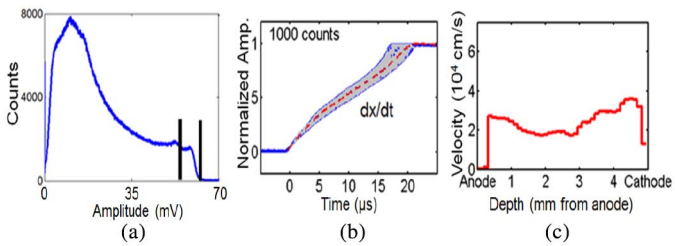

Fig. 2. (a) Cathode spectrum and window isolating cathode-side photopeak events. (b) The normalized average cathode waveform of windowed events is shown as the dashed trace. (c) The calculated electron drift velocity profile.

was used to ensure precise temperatures. For most cases, the detectors were cathode biased to −1000V and flood irradiated with ^{137}Cs to test the gamma response. Due to the small active volume of the detector and limited data transfer rate of the GageScope, gamma-ray measurements were analyzed in twenty-four-hour data sets.

B. Digital Pulse Processing

The amplitudes of all ten waveforms (nine anode pixels and cathode) were determined using simple subtraction (see Fig. 1). One-hundred sampling points were used for the baseline and tail averages. The gamma-ray spectra were corrected for electron trapping and weighting potential effects (both depth dependent) using the cathode-to-anode-ratio (CAR) [12]. The CAR was also used to determine the depth-dependent photopeak count rates.

C. Determination of Drift Velocity

Cathode waveforms from cathode-side photopeak events were used to determine the depth-dependent electron drift velocity. These events were selected by windowing on the upper end of the cathode spectrum, as shown in Fig. 2(a). Once the cathode-side photopeak events were isolated, the waveforms were normalized to account for any amplitude differences. (Typical energy resolutions ranged from 1 to 3% FWHM at 662 keV; therefore photopeak events do not have the exact same amplitude.) Because of the linear cathode weighting potential, a change in cathode amplitude is proportional to a change in depth. The depth-dependent drift velocity was calculated by dividing the change in cathode signal amplitude by the change in time for each of twenty or forty cathode-signal depth bins (see Fig. 2(b)–(c)). A similar method using alpha particles has previously been applied to TlBr and CZT detectors and the results are consistent with that of electrons [3], [13].

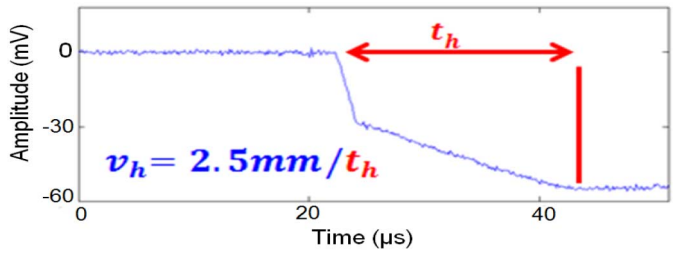

Fig. 3. Sample waveform from a center event used to calculate the hole drift time for high hole mobility detectors.

D. Special Case for Hole Drift Velocity

Some TlBr detectors show a relatively high hole mobility and full hole collection is observed for photopeak interactions in the center of the detector. Fig. 3 shows a center event for a typical detector with high hole mobility. The first slope ($22\ \mu s < t < 26\ \mu s$) is caused by the drift of both electrons and holes. The second slope ($26\ \mu s < t < 42\ \mu s$), is caused by the drift of only holes. The electrons are fully collected at $t = 26\ \mu s$ due to a faster drift velocity, resulting in the observed kink in the waveform. The hole drift velocity was estimated by isolating center events ($0.48 < \mathrm{CAR} < 0.52$) and dividing half the detector thickness (2.5 mm) by the hole drift time. Unlike the electron drift velocity, this method only estimates an average value instead of a depth-dependent drift velocity profile.

E. Determination of Freed Electron Concentration

The freed electron concentration was estimated by measuring the change in leakage current through the pixel preamplifiers after the sample was illuminated with a Cree, Inc. 2.1 eV (sub-bandgap) through-hole LED. The current was determined by measuring the DC offset of the feedback resistor, the only DC path through the preamplifier. A detailed description of the leakage current measurement (without LED stimulation) can be found in Ref. [11]. When the LED is turned on, sub-bandgap photons excite trapped electrons into the conduction band, increasing the leakage current. The impulse current in each pixel is given by Eq. (1):

$$\Delta I = \Delta n v_e q A \tag{1}$$

where Δn is the conduction band population increase (i.e. concentration of freed (detrapped) electrons), v_e is the electron drift velocity, q is the electron charge, and A is the pixel pad area. Rearranging Eq. (1) results in an expression for the freed electron concentration as a result of the LED illumination:

$$\Delta n = \Delta I / v_e q A. \tag{2}$$

For detectors with low $\mu_h \tau_h$ compared to $\mu_e \tau_e$, the hole drift velocity will be negligible compared to the electron drift velocity and the current will be dominated by freed electrons and not freed holes. Based on gamma-ray analysis, this was the case for detectors 935-16B1L and 44B2L, but not detector 935-

35AA1L. As a result, this method was not applied to detector 935-35AA1L.

The LED was used to illuminate the detector before each twenty-four-hour data acquisition and the impulse current, ΔI, was measured in each pixel. The impulse current was proportional to the LED current up to $\sim$ 13 mA. To ensure the same LED current (photon flux) each day, the impulse was measured for three LED currents ($\sim$ 3 mA, $\sim$ 6 mA, and $\sim$ 9 mA) and a linear best-fit line was used to determine the expected impulse at exactly 6 mA. The uncertainty in the calculated impulse at 6 mA (derived from the uncertainties in the linear fit parameters) was propagated to the freed electron concentration uncertainties.

Waveforms from the first hour following the LED stimulation were used to estimate the electron drift velocity using techniques described in Section II-C. The LED was turned off during the gamma-ray data acquisition. Previous work has used light stimulation to remove space charge from TlBr [14] and even measure electron concentrations of solar cell semiconductor materials [15], [16]. The novelty of our approach is that the same experimental setup (no change in bias, temperature, electrode configuration, etc.) is used to measure the change in trapped electrons and detector performance (energy resolution, electric field profiles), simultaneously.

III. Results

A. Electric Field Stabilization

Previous work has shown that the electron drift velocity increases and becomes more uniform during the conditioning phase [3], [17]. It was unclear whether the improvement was due to a stronger effective electric field or higher mobility ($v_e = E*\mu_e$). (Note that while the spatial average electric field is set by the detector bias, there is no such constraint on the average drift velocity. The average drift velocity will dramatically increase ($>$ 2x) when the electric field becomes more uniform. Therefore, it is useful to define the effective average electric field:

$$E_{eff} =< v_d > /\mu_e. \tag{3}$$

E_{eff} is not constrained by the detector bias and will increase when the true electric field becomes more uniform.) Detector 935-35AA1L had sufficient hole mobility to measure both the electron and hole drift velocities. Fig. 4 shows the hole drift velocity as a function of the electron drift velocity during the conditioning phase.

The linearity in Fig. 4 suggests that either the mobilities are increasing by the same percentage, or the effective electric field is increasing. Because the mobilities of holes and electrons are governed by properties of the valence band and conduction band respectively, it is unlikely that the mobilities would happen to change by the exact same percentage during conditioning. It is more likely that the effective electric field is increasing, resulting in the simultaneous improvement of both the electron and hole drift velocities. The slope of the least squares best-fit line in Fig. 4 gives the mobility ratio: $m = \mu_h/\mu_e = 0.15$. This ratio is higher than what is observed for most TlBr detectors and indicates that high hole mobility crystals are achievable, allowing for the possibility of simple planar electrodes.

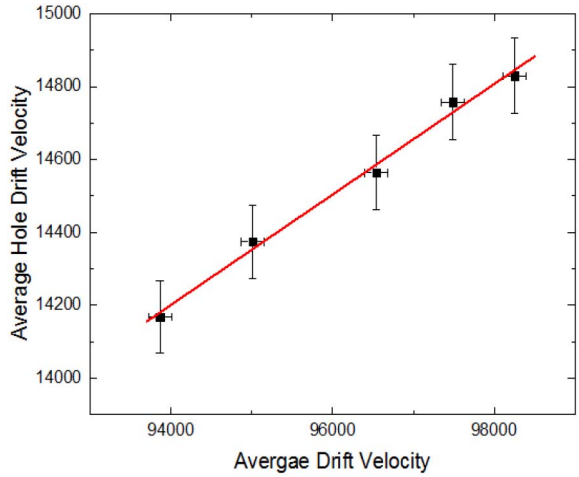

Fig. 4. Hole drift velocity as a function of the electron drift velocity for detector 935-35AA1L at 2000 V. The least squares line of best fit has the following parameters: Slope $= 0.151 \pm 0.007$, Intercept $= 60 \pm 700$, $r^2 = 0.991$.

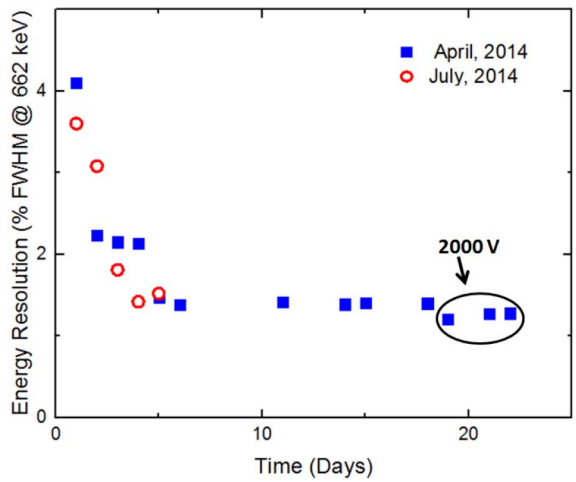

Fig. 5. Time-dependent energy resolution for detector 935-16B1L during two different conditionings.

B. Spectroscopy, Active Volume, and The Role of Trapped Electrons

Each TlBr detector conditioned at the University of Michigan demonstrated unique behavior. Two detectors were studied using slightly different procedures in order to fully quantify the conditioning phase.

1) Detector 935-16B1L: Detector 935-16B1L was conditioned at $-20°$C in April 2014. It was subsequently biased down, warmed up to room-temperature, stored in a desiccator for three months, and reconditioned at $-20°$C in July 2014. The time-dependent energy resolution for both tests is shown in Fig. 5. Each twenty-four hour dataset had more than four hundred and fifty thousand photopeak counts so the FWHM uncertainty is negligible. In both measurements, the energy resolution improves dramatically over the first five days, indicating that whatever mechanism causes the improvement, relaxes when the detector is stored without bias.

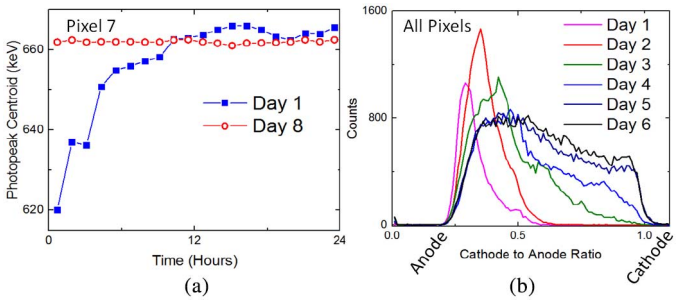

Fig. 6. (a) Photopeak centroid as a function of time over day one (solid squares) and day eight (open circles). (b) Total photopeak counts as a function of depth during conditioning.

The photopeak centroid (proportional to charge collection efficiency) as a function of time during day one and day eight is shown in Fig. 6(a). Based on the energy resolution and number of photopeak counts, the centroid uncertainties are on the order of 0.03% and unobservable on the figure. On day one, the photopeak centroid is very unstable, artificially degrading the energy resolution. On day eight, the centroid is stable and good energy resolution is observed.

In contrast to detector 935-35AA1L, detector 935-16B1L did not have significant hole transport and the hole drift velocity could not be measured. Over the first six days of both the April 2011 and July 2011 conditionings, the average electron drift velocity improved from less than $2x10^4$ cm/s (minimum measureable drift time given the sampling window) to $\sim 7.5x10^4$ cm/s. Based on results from Fig. 4 (a different detector with high hole mobility), it is likely here to that the electron drift velocity increase is caused by an increase in the effective electric field (as opposed to the mobility).

Fig. 6(b) shows the photopeak counts (raw anode amplitude between 1200 ADC and 1500 ADC) as a function of depth (from CAR) over the first six days of the April 2014 conditioning. On the first day, photopeak counts are recorded only within ~ 2 mm of the anode surface, indicating that the internal electric field is very weak in the center of the detector. Electron clouds from both cathode-side and center events must travel through the weak electric field in the center of the detector before being collected by the anode. Therefore, even though the electric field is likely high near the cathode (in order to preserve the average electric field set by the cathode bias), no photopeak events are observed near the cathode. The low electric field in the center causes a poor region in the center and cathode side where increased trapping and poor charge-collection-efficiency occurs, removing photoelectric interactions from the photopeak range defined above (1200 to 1500 ADC). As the device conditions and the electric field improves, the fraction of the detector with poor charge-collection-efficiency decreases from $\sim 60\%$ on day one, to $\sim 50\%$ on day 2, to $\sim 30\%$ on day 3, and to $\sim 5\%$ on day 4. The energy resolution shows a sharp improvement between day four and day five (see solid squares in Fig. 5) corresponding to when the poor region disappears.

Due to the slow cathode rise time, the exact electric field profile could not be measured during the first three days. However, by day four, the entire cathode waveform was collected in the sampling window and the drift velocity profile was calculated using the method described in Section II-C. Using the known 2000 V/cm average electric field to normalize the profile, the depth dependent electric field was estimated from the drift velocity profile for day four (see Fig. 7). Photopeak events were observed at all depths for the first time on day four (see Fig. 6(b)). Therefore, the electric field in the center must have been greater than a critical value required to observe photopeak events at all depths in detector 935-16B1L. The minimum electric field on day four was $\sim$ 1000 V/cm, which provides an

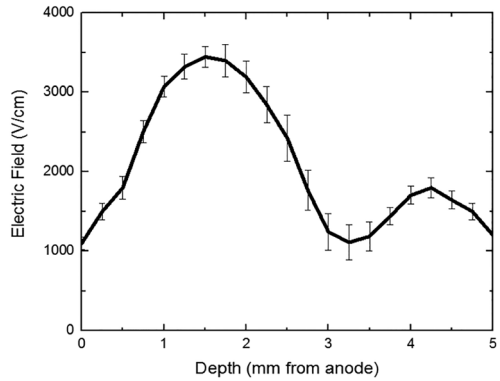

Fig. 7. Electric field profile for the fourth day of the April 2014 conditioning of detector 935-16B1L. The minimum electric field value sets an upper limit on the critical electric field required to observe photopeak events at all depths.

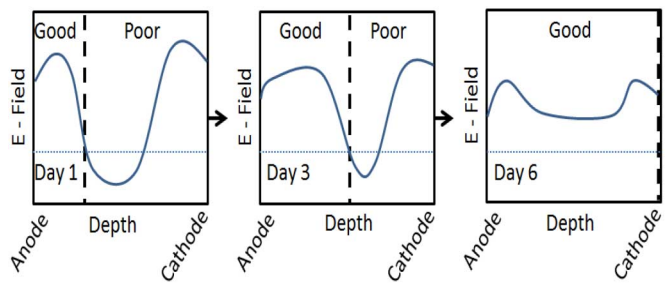

Fig. 8. Cartoon of the electric field profile in detector 935-16B1L during the conditioning phase. The horizontal dotted line represents a critical electric field that has to be achieved in order to observe photopeak counts. The vertical dashed line separates the good region (observable photopeak counts) from the poor region (no observable photopeak counts).

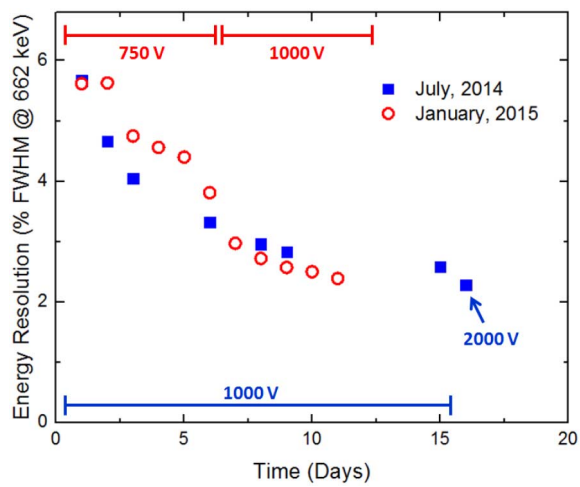

Fig. 9. Time-dependent energy resolution for detector 44B2L during two different conditionings.

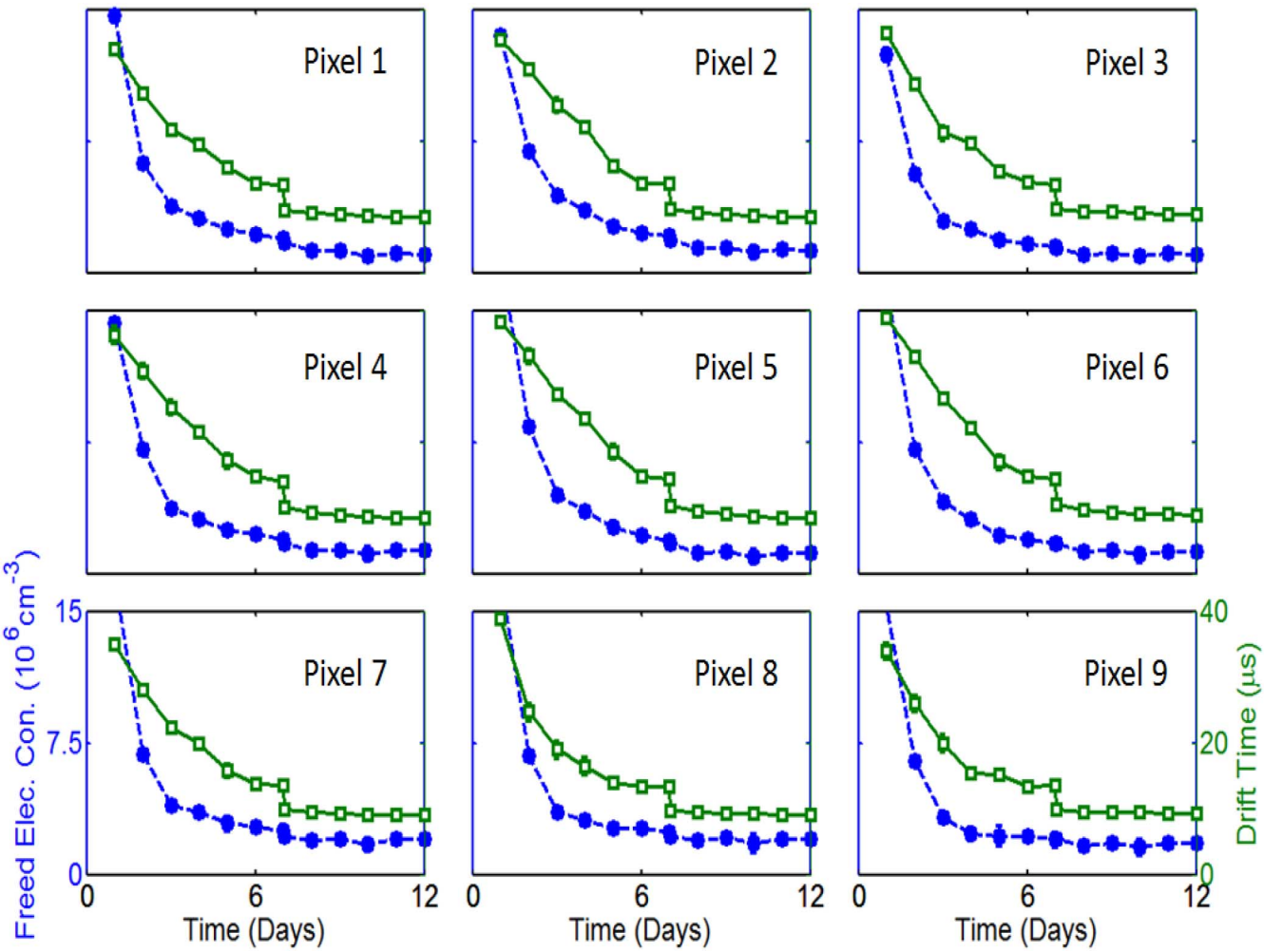

Fig. 10. Freed electron concentration (solid circle) and cathode-side drift time (open squares) for the January 2015 conditioning in each pixel of detector 44B2L. The discontinuity in the drift time occurs because the bias was increased from 750 V to 1000 V.

upper bound for this critical electric field. For days prior to day 4, the electric field in the center of the detector must have been below 1000 V/cm since photopeak counts were not recorded at all depths.

Although the cathode side drift time was too slow to calculate the drift velocity profile during the first three days, Figs. 6(b) and 7 were used to create a cartoon of the expected electric field during all parts of the conditioning phase (see Fig. 8). The horizontal dotted line shows the critical electric field ($\sim$ 1000 V/cm) that must be achieved in the center of the detector in order to observe photopeak events at all depths.

2) Detector 44B2L: Detector 44B2L was also conditioned two separate times to verify the relaxation of the conditioning mechanism. Fig. 9 shows the time-dependent energy resolution for July 2014 and January 2015 measurements. Each twenty-four hour spectrum had more than four hundred and eighty thousand photopeak counts so the FWHM uncertainty is negligible. During the January 2015 condition, the bias was increased from 750 V to 1000 V after six days. When the bias was 750 V, the January 2015 improvement was slower compared to the July 2014 improvement. After the bias was increased, the conditioning in January 2015 was faster compared to July 2014, indicating that a higher bias can speed up the conditioning phase.

Before each twenty-four-hour measurement during the January 2015 conditioning, an LED was used to illuminate the detector and the concentration of freed electrons from the LED photons was estimated using Eq. (2). Fig. 10 shows the freed electron concentration and cathode-side-event electron drift-times for each pixel during the January 2015 conditioning phase. The uncertainties are on the order of 4 to 6% and are not visible for some points. The freed electron concentration is the number of detrapped electrons as a result of exactly 6 mA of current through the interrogating LED. The resulting number of photons is well below the number required to free all trapped electrons. Therefore, the freed electron concentration shown in Fig. 10 is proportional, but not equal, to the total number of trapped electrons. The proportionality constant was maintained from day to day by using the same current (number of photons) though the LED. As expected, there is a discontinuity in the day 7 drift-times (open squares in Fig. 10) when the bias was increased from 750 V to 1000 V. The freed electron concentration is independent of the electric field, so no discontinuity is observed (solid circles in Fig. 10).

The freed electron concentration and drift time (an inverse measure of the effective electric field) decrease continuously in all pixels to less than a fifth of their original values. During the conditioning phase, the number of trapped electrons decreases, either because the concentration of filled traps decreases from photon and LED excitation, or because the number of trapping sites is lowered as charged impurities drift to the electrode and are neutralized. In the latter case, lowering the impurity concentration of the bulk material would shorten the conditioning phase. In either case, the total amount of trapped space charge is reduced, resulting in a more uniform internal electric field. From Fig. 10, the effective average electric field improves by more than 3x as a result of a more than 4x space charge reduction. The spectroscopy is dependent on the uniformity of the electric field and improves from 5.6% to 2.4% as a result of the reduced space charge.

IV. Conclusions

Conditioning occurs in some TlBr detectors operated at $-20°C$. The energy resolution and electron drift velocity improve over time. By measuring the electron and hole drift velocities simultaneously, we conclude that the improved drift velocity is the result of a more uniform electric field and not a higher mobility. Additionally, we found that the uniform electric field results in a stable photopeak and better energy resolution. A new technique using LED stimulation was developed to monitor the freed electron concentration with the same setup used to measure performance characteristics. The results showed the influence of trapped space charge on detector performance. It is likely that the space charge reduction over time improved the electric field uniformity. From these results, we conclude that reducing the impurity concentration which leads to trapped space charge, would shorten the conditioning time.

Conditioning the detectors multiple times at different biases showed that the conditioning mechanism relaxes when the detector is not at bias and that the conditioning speed is dependent upon the applied bias. Therefore, a higher bias can be applied to condition the detector more quickly. After the device conditions, the bias can be lowered for normal operation.

Based on these results, we expect that operating the detector at higher temperatures would decrease the conditioning time because the trapped space charge would either migrate more quickly (in the case of charged impurities) or be freed from thermal excitations (in the case of trapped electrons). However, increasing the temperature increases the probability of polarization.

References

[1] A. V. Churilov, W. M. Higgins, G. Ciampi, H. Kim, L. J. Cirignano, F. Olschner, and K. S. Shah, "Purification, crystal growth and detector performance of TlBr," *Proc. SPIE*, vol. 7079, pp. K1–K8, 2008.

[2] H. Kim, L. Cirignano, A. Churilov, G. Ciampi, W. Higgins, F. Olschner, and K. Shah, "Developing larger TlBr detectors: Detector performance," *IEEE Trans. Nucl. Sci.*, vol. 56, no. 3, pp. 819–823, Jun. 2009.

[3] C. Thrall, W. Kaye, Z. He, H. Kim, L. Cirignano, and K. Shah, "Transient behavior in TlBr gamma-ray detectors and its analysis using 3-d position sensing," *IEEE Trans. Nucl. Sci.*, vol. 60, no. 2, pp. 1162–1167, Apr. 2013.

[4] K. Hitomi, Y. Kikuchi, T. Shoji, and K. Ishii, "Improvement of energy resolutions in TlBr detectors," *Nucl. Instrum. Methods Phys. Res. A*, vol. 601, pp. 112–115, Aug. 2009.

[5] K. Hitomi, T. Shoji, and K. Ishiir, "Advances in TlBr detector development," *J. Cryst. Growth*, vol. 379, pp. 93–98, 2013.

[6] K. Hitomi, T. Onodera, S. Kim, T. Shoji, and K. Ishii, "Characterization of pixelated TlBr detectors with Tl electrodes," *Nucl. Instrum. Methods Phys. Res. A*, vol. 747, pp. 7–12, Feb. 2014.

[7] B. Donmenz, Z. He, H. Kim, L. J. Cirignano, and K. S. Shah, "The stability of TlBr detectors at low temperature," *Nucl. Instrum. Methods Phys. Res. A*, vol. 623, no. 3, pp. 1024–1029, 2010.

[8] K. Hitomi, T. Shoji, and Y. Niizeki, "A method for suppressing polarization phenomena in TlBr detectors," *Nucl. Instrum. Methods Phys. Res. A*, vol. 585, pp. 102–104, Jan. 2008.

[9] A. Conway, L. Voss, A. Nelson, P. Beck, T. Laurence, R. Graff, R. Nikolic, S. Payne, H. Kim, L. Cirignano, and K. Shah, "Fabrication methodology of enhanced stability room temperature TlBr gamma detectors," *IEEE Trans. Nucl. Sci.*, vol. 60, no. 2, pp. 1231–1236, Apr. 2013.

[10] V. Kozlov, M. Kemell, M. Vehkamaki, and M. Leskela, "Degradation effects in TlBr single crystals under prolonged bias voltage," *Nucl. Instrum. Methods Phys. Res. A*, vol. 576, pp. 10–14, Jun. 2007.

[11] W. Koehler, Z. He, C. Thrall, S. O'Neal, H. Kim, L. Cirignano, and K. Shah, "Quantitative investigation of room-temperature breakdown effects in pixelated TlBr detectors," *IEEE Trans. Nucl. Sci.*, vol. 60, no. 2, pp. 2573–2578, Apri. 2013.

[12] Z. He, W. Li, G. Knoll, D. Wehe, J. Berry, and C. Stahle, "3-d Position sensitive CdZnTe gamma-ray spectrometers," *Nucl. Instrum. Methods Phys. Res. A*, vol. 442, no. 13, pp. 173–198, 1999.

[13] J. C. Kim, W. R. Kaye, W. Wang, F. Zhang, and Z. He, "Impact of drift time variation on the Compton image from large-volume CdZnTe crystals," *Nucl. Instrum. Methods Phys. Res. A*, vol. 683, pp. 53–62, 2012.

[14] I. Rahman and R. Hofstadter, "Thallium halide radiation detectors," *Phys. Rev. B*, vol. 29, no. 6, pp. 3500–3507, 1984.

[15] Q. Wang, S. Ito, M. Gratzel, F. Fabregat-Santiago, I. Mora-Sero, J. Bisquert, T. Bessho, and H. Imai, "Characteristics of high efficiency dye-sensitized solar cells," *J. Phys. Chem. B*, vol. 110, pp. 25210–25221, 2006.

[16] J. Bisquert, F. Fabregat-Santiago, I. Mora-Sero, G. Garcia-Belmonte, and S. Gimenez, "Electron lifetime in dye-sensitized solar cells: Theory and interpretation of measurements," *J. Phys. Chem. B*, vol. 113, pp. 17278–17290, 2009.

[17] C. Thrall, "Alternative wide-band-gap materials for gamma-ray spectroscopy," Ph.D. dissertation, Univ. of Michigan, Ann Arbor, MI, USA, 2013.